Nonadiabatic reaction rates for dissipative quantum-classical systems

Alessandro Sergi and Raymond Kapral
Chemical Physics Theory Group, Department of Chemistry, University of Toronto, Toronto, Ontario M5S 3H6, Canada

(Received 27 August 2003; accepted 26 September 2003)

The dynamics of a quantum system which is directly coupled to classical degrees of freedom is investigated. The classical degrees of freedom are in turn coupled to a classical bath whose detailed dynamics is not of interest. The resulting quantum-classical evolution equations are dissipative as a result of coupling to the classical heat bath. The dissipative quantum-classical dynamics is used to study nonadiabatic chemical reactions and compute their rates. The reactive flux correlation formalism for the calculation of nonadiabatic rate constants is generalized to dissipative quantum-classical dynamics and implemented in terms of averages over surface-hopping Langevin trajectory segments. The results are illustrated for a simple quantum-classical two-state model. The techniques developed in this paper can be applied to complex classical environments encountered, for example, in proton and electron transfer processes in the condensed phase where local environmental degrees of freedom must be treated explicitly but the remainder of the environment can be treated simply as a heat bath. © *2003 American Institute of Physics.*
[DOI: 10.1063/1.1627752]

I. INTRODUCTION

There are many instances where chemical reactions are intrinsically quantum in nature but the environment in which they occur can be treated classically to a good approximation. For instance, in signalling processes in biomolecules the primary events often involve phenomena taking place on the quantum level, such as photon absorption leading to promotion to an excited electronic state. Successive reaction steps typically involve a classical flow of information to larger scales where dissipation is an essential ingredient in the passage back to the initial state. Proton and electron transfer reactions are often strongly influenced by the local media in which they occur, with the remainder of the degrees of freedom characteristic of the system providing a dissipative environment for the reactive dynamics. These considerations motivate the study of quantum-classical dynamics in dissipative baths where a portion of the system is treated quantum mechanically, its immediate surroundings is treated classically in full detail and the remainder of the environment is treated as a stochastic dissipative medium. For systems of this type one would like to investigate the microscopic nature of the quantum reactive dynamics and compute the reaction rate constants. These issues are discussed in this paper.

A variety of techniques can be used to study quantum dissipative dynamics (see Refs. 1 and 2 and references therein). Path-integral influence functional techniques[3,4] and imaginary time path integrals with analytic continuation through maximum entropy methods[5] have been used to compute rate constants for quantum dissipative systems. Rate constants have also been computed using the golden rule formula with time evolution treated by means of mean-field, semiclassical stochastic dynamics[6] and through the evaluation of the flux–flux correlation function expressions for the rate constant by means of surface-hopping schemes.[7]

We utilize the formulation of quantum-classical dynamics based on a quantum-classical Liouville equation and its representation in terms of surface-hopping trajectories.[8] The statistical mechanics of such quantum-classical systems has been developed[9] so that the rate constants can be computed from reactive flux autocorrelation functions *in situ* ations where nonadiabatic effects are important.[10] In this paper we extend this approach to the simulation of nonadiabatic quantum-classical dynamics to situations where part of the classical bath is described by dissipative stochastic dynamics.

Dissipative quantum-classical dynamics bath can be considered as a particular form of an open quantum system.[11,12] The equations of motion for such dynamics which we employ have been derived from the quantum-classical Liouville equation by means of projection operator techniques,[13] and take the form of a quantum-classical Fokker–Planck equation for the density matrix. We show how the time evolution of such a system can be represented by means of surface-hopping trajectory segments described by stochastic Langevin dynamics. This is the most convenient form of the dynamics for large scale numerical studies. To illustrate the method we compute the reaction rates for a simple two-level model. The model is similar to that used previously to investigate nonadiabatic reaction dynamics in quantum-classical systems,[10] except that now part of the classical environment is treated stochastically.

The paper is organized as follows: In Sec. II we introduce quantum-classical dynamics in a dissipative bath described by a Fokker–Planck equation of motion for the density matrix and its associated Kramers operators. In Sec. III we show how to map the dissipative evolution to an average over different realizations of Langevin trajectories. In Sec. IV we introduce the model system used to illustrate the for-

malism, give the expressions for the time-dependent rate coefficients, and discuss the equilibrium density matrix. In Sec. V we describe the simulation method, which generalizes the sequential short-time propagation algorithm[14] to the case of explicitly time-dependent propagators and, in Sec. VI present the results of our computation of the nonadiabatic rate constants. Section VII contains the conclusions of our study. The general proof of existence of a stationary density matrix for quantum-classical dynamics in a dissipative bath is given in the Appendix.

II. QUANTUM-CLASSICAL DYNAMICS IN A STOCHASTIC BATH

Consider a quantum-classical system comprising a quantum subsystem and a classical environment. The classical environmental phase space degrees of freedom are partitioned into two sets: one set (R,P) is directly coupled to the quantum subsystem and the details of its dynamics is necessary for an accurate description of the system dynamics; the second set (R',P') is coupled directly to the first set of classical degrees of freedom and its main effect is to function as a thermal bath leading to dissipative dynamics in the system.[13]

An equation of motion for the quantum-classical system composed of the quantum subsystem and the classical (R,P) degrees of freedom only has been derived using projection operator methods.[13] It takes the form

$$\frac{\partial\hat{\rho}_W(t)}{\partial t}=-\frac{i}{\hbar}[\hat{H}_W,\hat{\rho}_W(t)]+\frac{1}{2}(\{\hat{H}_W,\hat{\rho}_W(t)\}-\{\hat{\rho}_W(t),\hat{H}_W\})+\zeta\frac{\partial}{\partial P}\left(\frac{P}{M}+k_BT\frac{\partial}{\partial P}\right)\hat{\rho}_W(t)=-i\hat{\mathcal{L}}^D\hat{\rho}_W(t), \tag{1}$$

where ζ is the friction constant and k_BT is the Boltzmann constant times the temperature. The Hamiltonian

$$\hat{H}_W=\frac{P^2}{2M}+\frac{\hat{p}^2}{2m}+\hat{\mathcal{V}}_W(\hat{q},R)=\frac{P^2}{2M}+\hat{h}_W(R) \tag{2}$$

depends only on the (R,P) phase space coordinates and contains $\hat{\mathcal{V}}_W(\hat{q},R)$, the potential of mean force resulting from the average over the primed bath variables. The quantum and classical degrees of freedom have mass m and M, respectively, with $m\ll M$. The last equality in Eq. (1) defines the Liouville operator $i\hat{\mathcal{L}}^D$ determining the dissipative dynamics of the system. The dissipative quantum-classical Liouville operator in Eq. (1) differs from that derived for an isolated quantum-classical system[8] by the presence of the Fokker–Planck-type operator and the renormalized potential of mean force in the Hamiltonian.

The dissipative Liouville operator can be written in the adiabatic basis, being defined by the solution of the eigenvalue problem $\hat{h}_W|\alpha;R\rangle=E_\alpha(R)|\alpha;R\rangle$, as

$$-i\hat{\mathcal{L}}^D_{\alpha\alpha'\beta\beta'}=-[i\omega'_{\alpha\alpha'}(R)+iL^K_{\alpha\alpha'}]\delta_{\alpha\beta}\delta_{\alpha'\beta'}+J_{\alpha\alpha'\beta\beta'}, \tag{3}$$

where we have defined the Kramers operator as

$$iL^K_{\alpha\alpha'}=\left[\frac{P}{M}\frac{\partial}{\partial R}+\frac{1}{2}(\mathcal{F}^\alpha_W+\mathcal{F}^{\alpha'}_W)\cdot\frac{\partial}{\partial P}-\zeta\frac{\partial}{\partial P}\left(\frac{P}{M}+k_BT\frac{\partial}{\partial P}\right)\right], \tag{4}$$

where $\mathcal{F}^\alpha_W=-\partial\mathcal{V}^\alpha_W/\partial R$ denotes the effective Hellmann–Feynman force acting on the relevant variables. The operator J, giving rise to nonadiabatic transitions and corresponding bath momentum changes, has the same form as in earlier studies[8,15,10] and is given by

$$J_{\alpha\alpha'\beta\beta'}=-\frac{P}{M}\cdot d'_{\alpha\beta}\left(1+\frac{1}{2}S_{\alpha\beta}\cdot\frac{\partial}{\partial P}\right)\delta_{\alpha'\beta'}-\frac{P}{M}\cdot d^*_{\alpha'\beta'}\left(1+\frac{1}{2}S^*_{\alpha'\beta'}\cdot\frac{\partial}{\partial P}\right)\delta_{\alpha\beta}, \tag{5}$$

where $S_{\alpha\beta}=\Delta E_{\alpha\beta}[(P/M)\cdot\hat{d}_{\alpha\beta}]^{-1}$.

The quantum-classical average of any operator or dynamical variable $\hat{\chi}$ can be written as

$$\langle\hat{\chi}\rangle(t)=\sum_{\alpha\alpha'\beta\beta'}\int dRdP\chi_{\alpha'\alpha}(R,P)\times\exp[-i\mathcal{L}^D_{\alpha\alpha'\beta\beta'}t]\rho_W^{\beta\beta'}(R,P)=\sum_{\alpha\alpha'\beta\beta'}\int dRdP\rho_W^{\beta\beta'}(R,P)\times\exp[i\mathcal{L}^{DB}_{\beta'\beta\alpha'\alpha}t]\chi_{\alpha'\alpha}(R,P), \tag{6}$$

where $i\mathcal{L}^{DB}_{\beta'\beta\alpha'\alpha}$ is the backward operator that can be obtained by integrating by parts and using cyclic permutations under the trace. The explicit expression for the backward operator is

$$i\hat{\mathcal{L}}^{DB}_{\alpha\alpha'\beta\beta'}=[i\omega'_{\alpha\alpha'}(R)+iL^{KB}_{\alpha\alpha'}]\delta_{\alpha\beta}\delta_{\alpha'\beta'}-J_{\alpha\alpha'\beta\beta'}, \tag{7}$$

where the backward Kramers operator

$$iL^{KB}_{\alpha\alpha}=\left[\frac{P}{M}\frac{\partial}{\partial R}+\frac{1}{2}(\mathcal{F}^\alpha_W+\mathcal{F}^{\alpha'}_W)\cdot\frac{\partial}{\partial P}-\zeta\left(\frac{P}{M}-k_BT\frac{\partial}{\partial P}\right)\frac{\partial}{\partial P}\right]\delta_{\alpha\beta}\delta_{\alpha'\beta'}. \tag{8}$$

III. LANGEVIN DYNAMICS

From the classical theory of random processes[16] the time evolution under the backward Kramers operator $i\mathcal{L}^{KB}_{\alpha\alpha'\beta\beta'}$ can be replaced by an average over realizations of stochastic Langevin dynamics. In this representation the time evolution of the classical trajectory segments is determined by the Langevin equations of motion,

$$\dot{R}=\frac{P}{M}, \tag{9}$$

$$\dot{P}=-\frac{\zeta}{M}P+\frac{1}{2}(\mathcal{F}^\alpha_W+\mathcal{F}^{\alpha'}_W)+\xi(t), \tag{10}$$

where $\xi(t)$ is a Gaussian white-noise process with the properties

$$\langle \xi(t) \rangle = 0, \tag{11}$$

$$\langle \xi(t)\xi(t') \rangle = 2k_B T \zeta \delta(t-t'). \tag{12}$$

We can associate a time-dependent Liouville operator,

$$iL^L_{\alpha\alpha'}(t) = \frac{P}{M}\frac{\partial}{\partial R} + \left(-\frac{\zeta}{M}P + \frac{1}{2}(\mathcal{F}^\alpha_W + \mathcal{F}^\alpha_W) + \xi(t) \right)\frac{\partial}{\partial P}, \tag{13}$$

and a time-ordered propagator,

$$U^L_{\alpha\alpha'}(t,0) = \mathcal{T}\exp\left[\int_0^t dt' iL^L_{\alpha\alpha'}(t') \right], \tag{14}$$

with Eqs. (9) and (10). Consequently one is led to consider a total time-dependent Langevin–Liouville operator,

$$i\hat{\mathcal{L}}^L_{\alpha\alpha'\beta\beta'}(t) = [i\omega_{\alpha\alpha'}(R') + iL^L_{\alpha\alpha'}(t)]\delta_{\alpha\beta}\delta_{\alpha'\beta'} - J_{\alpha\alpha'\beta\beta'} \tag{15}$$

and the propagator

$$\mathcal{U}^L_{\alpha\alpha'\beta\beta'}(t,0) = \mathcal{T}\exp\left[\int_0^t dt' i\mathcal{L}^L_{\alpha\alpha'\beta\beta'}(t') \right]. \tag{16}$$

In this Langevin representation, the quantum-classical average of $\hat{\chi}$ can be written as

$$\langle \hat{\chi} \rangle(t) = \sum_{\alpha\alpha'\beta\beta'} \int dR dP \rho^{\beta\beta'}_W(R,P) \times \overline{\mathcal{U}^L_{\beta\beta'\alpha\alpha'}(t)\chi_{\alpha'\alpha}(R,P)}, \tag{17}$$

where the over line stands for an average over the different realizations of the Langevin stochastic process. We can permute the order of the average over phase space and over the stochastic process given by ξ since they are independent from each other. So we can write

$$\langle \hat{\chi} \rangle(t) = \sum_{\alpha\alpha'\beta\beta'} \overline{\int dR dP \rho^{\beta\beta'}_W(R,P)\mathcal{U}^L_{\beta\beta'\alpha\alpha'}(t)\chi'_{\alpha'\alpha}(R,P)}. \tag{18}$$

Equation (18) expresses dissipative quantum-classical averages as phase space weighted averages over different realizations of Langevin trajectories and is in a form that is convenient for numerical simulations.

IV. MODEL SYSTEM

To illustrate the formalism we consider a quantum two-level system which is directly coupled to a classical quartic oscillator; this quartic oscillator is in turn coupled to a dissipative bath. The Hamiltonian of the model is

$$\hat{H}_W(R,P) = \frac{P^2}{2M} + V_q(R) - \hbar\Omega\hat{\sigma}_x - \hbar\gamma_0 R\hat{\sigma}_z, \tag{19}$$

where $V_q(R) = (a/4)R^4 - (b/2)R^2$ and $\hat{\sigma}_x$ and $\hat{\sigma}_z$ are Pauli matrices. Henceforth we use dimensionless coordinates $\tilde{R} = (M\omega_c/\hbar)^{1/2}R$, $\tilde{p} = (\hbar M\omega_c)^{-1/2}P$, so that $\hat{\tilde{H}} = \hat{H}/(\hbar\omega_c)$. The dimensionless parameters of the model are $\tilde{\Omega} = \Omega/\omega_c$, $\tilde{a} = [\hbar/(M^2\omega_c^3)]a$, $\tilde{b} = b/(M\omega_c^2)$, $\tilde{\gamma}_0 = (\hbar/M\omega_c^3)^{1/2}\gamma_0$ while the dimensionless reciprocal temperature and time are $\tilde{\beta} = \hbar\omega_c\beta = \hbar\omega_c/k_BT$ and $\tilde{t} = t\omega_c$, respectively. We also define a dimensionless friction constant $\tilde{\zeta} = \zeta/M\omega_c$. Here ω_c is some characteristic frequency. In the following the tilde will be omitted to simplify the notation but the use of dimensionless units should be understood. The dimensionless parameters chosen for the calculation have the values $\Omega = 0.025$, $a = 3$, $b = 1.8$, and $\gamma_0 = 1$.

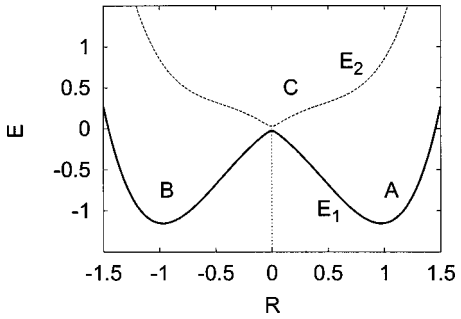

FIG. 1. Adiabatic energy surfaces of the model. The heavy solid line is the ground-state curve while the dashed line denotes the excited-state curve. The shapes of the energy curves suggest the definition of the three chemical species A, B, and C. Species A and B, reactant and product, are defined on the ground-state surface and they are separated by a vertical line at $R=0$. Species C is defined on the excited-state curve.

The Hamiltonian in Eq. (19) together with Eq. (1) completely specify the dynamics of the model. In the adiabatic basis the Hamiltonian takes the form $H^\alpha_W = P^2/2 + E_\alpha(R)$, where the adiabatic eigenvalues are given by

$$E_{1,2} = V_q(R) \mp \sqrt{\Omega^2 + \gamma_0^2 R^2}. \tag{20}$$

The adiabatic energy curves are shown in Fig. 1. The ground-state energy profile has two minima at $R = \pm 0.97$ separated by a barrier with height $\Delta V = 1.13$. The frequency at the barrier top is $\omega_b = 178.77$ while the frequency at the well minima is $\omega_0 = 2.49$.

From the shapes of the energy profiles in Fig. 1 one may define three chemical species A, B, and C which undergo the following chemical reactions:

$$A \underset{k_{BA}}{\overset{k_{AB}}{\rightleftharpoons}} B, \quad A \underset{k_{CA}}{\overset{k_{AC}}{\rightleftharpoons}} C, \quad B \underset{k_{CB}}{\overset{k_{BC}}{\rightleftharpoons}} C. \tag{21}$$

Due to mass conservation and detailed balance only two independent rate coefficients need to be computed. We choose to focus on the computation of k_{AB} and k_{AC}.

Time-dependent rate coefficients

Microscopic dynamical variables for the species operators A, B, and C may be defined as

$$\hat{N}_A = |1;R\rangle\Theta(R)\langle 1;R|,$$

$$\hat{N}_B = |1;R\rangle\Theta(-R)\langle 1;R|, \tag{22}$$

$$\hat{N}_C = |2;R\rangle\langle 2;R|,$$

where $\Theta(\pm R)$ is the Heaviside function selecting the right or left wells and $|1(2);R\rangle\langle 1(2);R|$ is a projector onto the

adiabatic state $|1(2);R\rangle$. Note that $\Sigma_{I=A}^{C}\hat{N}_I=1$, reflecting the fact that the combined Hilbert and configuration space is completely partitioned into regions corresponding to the three species.

The expressions for the time-dependent $k_{AB}(t)$ and $k_{AC}(t)$ rate constants were derived in Ref. 10 and are given by

$$k_{AB}(t)=-(\beta\overline{n}_A^{eq})^{-1}\mathrm{Tr}'\int dRdP\hat{\chi}_B(t)(\hat{\chi}_A,\hat{\rho}_{We}), \quad (23)$$

$$k_{AC}(t)=-(\beta n_A^{eq})^{-1}\mathrm{Tr}'\int dRdP\hat{\chi}_C(t)(\hat{\chi}_A,\hat{\rho}_{We}). \quad (24)$$

In Eqs. (23) and (24) we have used the quantum-classical bracket defined as $(\hat{\chi}_I,\hat{\rho}_{We})=i/\hbar[\hat{\chi}_I,\hat{\rho}_{We}]-1/2(\{\hat{\chi}_I,\hat{\rho}_{We}\}-\{\hat{\rho}_{We},\hat{\chi}_I\})$. The progress variable $\hat{\chi}_I$ is defined as the deviation of $\hat{N}_I$ from its equilibrium value and $\hat{\rho}_{We}$ is the stationary density of the dissipative quantum-classical dynamics (see the Appendix for a discussion).

The plateau value of these correlation function expressions can be used to compute k_{AB} and k_{AC}, thus determining the two independent rate constants in the problem. Representation of the species variables in the adiabatic basis gives $\hat{N}_A^{\alpha\alpha'}=\delta_{\alpha 1}\delta_{\alpha' 1}\Theta(R)$, $\hat{N}_B^{\alpha\alpha'}=\delta_{\alpha 1}\delta_{\alpha' 1}\Theta(-R)$, and $\hat{N}_C^{\alpha\alpha'}=\delta_{\alpha 2}\delta_{\alpha' 2}$. The progress variables $\hat{\chi}_A$ and $\hat{\chi}_C$ may be replaced by $\hat{N}_A$ and $\hat{N}_C$ when computing Eqs. (23) and (24). An explicit formula for the stationary density matrix for quantum-classical dissipative dynamics can be easily determined to order $\mathcal{O}(\hbar)$. In the adiabatic basis and in dimensionless units it is given by

$$\rho_{We}^{\alpha\alpha'}\approx\rho_{We}^{(0)\alpha}\delta_{\alpha\alpha'}-if_{We}^{\alpha\alpha'}(1-\delta_{\alpha\alpha'}). \quad (25)$$

Equation (25) gives also the decomposition of the density matrix into diagonal and off-diagonal parts. The off-diagonal part of the density matrix has the properties $\rho_{We}^{12}=(\rho_{We}^{21})^*$ and $\rho_{We}^{12}+\rho_{We}^{21}=0$. For the diagonal part one finds

$$\rho_{We}^{(0)\alpha\beta}(R,P)=Z^{-1}e^{-\beta H_W^{\alpha}}\delta_{\alpha\beta}, \quad (26)$$

with $Z=\Sigma_{\alpha=1}^{2}\int dRdP\exp[-\beta H_W^{\alpha}]$. For the off-diagonal part one gets

$$f^{\alpha\alpha'}(R,P)=\rho_{We}^{(0)\alpha}Pd_{\alpha\alpha'}\left(\frac{\beta}{2}(1+e^{-\beta E_{\alpha'\alpha}})+\frac{1-e^{-\beta E_{\alpha'\alpha}}}{E_{\alpha\alpha'}}\right), \quad (27)$$

with $\alpha,\alpha'=1,2$. The nonadiabatic coupling matrix element $d_{\alpha\alpha'}=\langle\alpha;R|\partial/\partial R|\alpha';R\rangle$ which, assuming that the adiabatic basis is real, has the properties $d_{11}=d_{22}=0$ and $d_{12}=-d_{21}$.

The diagonal and off-diagonal contributions to the density matrix can be substituted into the explicit form of the quantum-classical bracket in the adiabatic basis and the time-dependent rate coefficient in Eq. (23) can be decomposed into the sum of three contributions:

$$k_{AB}(t)=k_{AB}^{d}(t)+k_{AB}^{o1}(t)+k_{AB}^{o2}(t). \quad (28)$$

The diagonal part of the density matrix gives rise to the contribution

$$k_{AB}^{d}(t)=(\beta n_A^{eq})^{-1}\int dRdPN_B^{11}(R,P,t)\delta(R)\frac{\partial\rho_{We}^{11}}{\partial P}, \quad (29)$$

while the off-diagonal part of the density matrix yields the two terms

$$k_{AB}^{o1}(t)=(\beta n_A^{eq})^{-1}\int dRdP\,\mathrm{Im}\{N_B^{12}(R,P,t)\}\times\delta(R)\frac{\partial f_{We}^{12}}{\partial P}, \quad (30)$$

$$k_{AB}^{o2}(t)=-2(\beta n_A^{eq})^{-1}\int dRdP\,\mathrm{Re}\{N_B^{12}(R,P,t)\}\Theta(R)\times\beta d_{12}P\rho_{We}^{11}\frac{1-e^{-\beta E_{21}}}{\beta E_{12}}. \quad (31)$$

Equations (29)–(31) provide formulas to calculate the time-dependent rate coefficient $k_{AB}(t)$ from whose plateau value the rate constant k_{AB} may be determined.

A completely analogous set of formulas can be used to compute k_{AC} by replacing $N_B^{\alpha\alpha'}(t)$ by $N_C^{\alpha\alpha'}(t)$ in the above equations.

V. SIMULATION METHOD

The calculation of quantum-classical averages and correlation functions using the dynamics specified by the time-dependent Langevin–Liouville operator $i\mathcal{L}_{ss'}^{L}(t)$ in Eq. (15) and its associated propagator $\mathcal{U}_{ss'}^{L}(t)$ in Eq. (16) is no more complicated than that for deterministic quantum-classical dynamics.[10,14,15,17] A simulation scheme requires a procedure to sample phase space points and an integration scheme for the Langevin trajectories. The average over phase space and different realizations of the stochastic process can be performed independently. To calculate Eqs. (29) and (30) R is kept fixed at the barrier top. To calculate Eq. (31) R is sampled uniformly in the right well. In all cases the momentum P is sampled from a Boltzmann distribution.

An efficient way to simulate the quantum-classical dynamics is provided by the sequential short-time propagation algorithm.[14,17] To obtain the results below, we have applied this scheme within the momentum-jump approximation.[10,18,19] The sequential short-time propagation algorithm for time-independent propagators is described in detail elsewhere.[14,17] In the present case the propagator $\mathcal{U}_{ss'}^{L}(t)$ is defined as a time ordered product due to the explicit time dependence of $i\mathcal{L}_{ss'}^{L}(t)$. In the following we will show how the scheme of Refs. 14 and 17 can be extended to the more general time-dependent case using the formalism of Suzuki.[20] We will also describe how the numerical integration of the Langevin trajectories can be performed within Suzuki's framework.[20]

A. Sequential short-time propagation for time-dependent propagators

Dividing the time interval t into N segments with lengths $\Delta t_j=t_j-t_{j-1}$, the time-dependent propagator in Eq. (16) can be written as a time-ordered composition of evolu-

tion operators with time segments of arbitrary length. We suppose all the time segments have equal length Δt and it is sufficient to restrict the description of the algorithm to propagation in a single interval Δt. The propagation for $t=N\Delta t$ is achieved by the ordered concatenation of the single interval propagation steps. Thus, considering the propagator in Eq. (16) for a small time interval Δt, one can use Suzuki's result[20] where any ordered exponential can be expressed by an ordinary exponential operator in terms of a super-operator $\mathcal{I}$,

$$\mathcal{U}^L_{\alpha_{j-1}\alpha'_{j-1},\alpha_j\alpha'_j}(\Delta t,0)=(e^{\Delta t[i\mathcal{L}^L(t=0)+\mathcal{I}]})_{\alpha_{j-1}\alpha'_{j-1},\alpha_j\alpha'_j}. \tag{32}$$

The super-operator $\mathcal{I}$ is given by the following differential operator:

$$\mathcal{I}=\frac{\overleftarrow{\partial}}{\partial t}, \tag{33}$$

defined so that, given any two time-dependent operators or functions $F(t)$ and $G(t)$, one has

$$F(t)e^{\tau\mathcal{I}}G(t)=F(t+\tau)G(t); \tag{34}$$

i.e., $\mathcal{I}$ acts on whatever is on its left and does not affect functions on its right.[20] Assuming Δt is small we can use a symmetric Trotter factorization[21] in Eq. (32),

$$\begin{aligned}\mathcal{U}^L_{\alpha_{j-1}\alpha'_{j-1},\alpha_j\alpha'_j}(\Delta t,0)&=(e^{(\Delta t/2)\mathcal{I}}e^{\Delta t i\mathcal{L}^L(t=0)}e^{(\Delta t/2)\mathcal{I}})_{\alpha_{j-1}\alpha'_{j-1},\alpha_j\alpha'_j}\\&=(e^{\Delta t\mathcal{I}}e^{\Delta t i\mathcal{L}^L(\Delta t/2)})_{\alpha_{j-1}\alpha'_{j-1},\alpha_j\alpha'_j}.\end{aligned} \tag{35}$$

In the second line of Eq. (35) we must keep the operator $\exp[\Delta t\mathcal{I}]$ because, even if it no longer acts on $\exp[\Delta t i\mathcal{L}^L(\Delta t/2)]$, one has to take it into account when building the entire time-ordered concatenation of propagators to determine the propagation for the full time length t,

$$\mathcal{U}^L_{\alpha_0\alpha'_0,\alpha_N\alpha'_N}(t,0)=\sum_{(\alpha_1\alpha'_1)\cdots(\alpha_{N-1}\alpha'_{N-1})}\times\prod_{j=1}^{N}(e^{\Delta t i\mathcal{L}^L[(t_j-t_{j-1})/2]})_{\alpha_{j-1}\alpha'_{j-1},\alpha_j\alpha'_j}. \tag{36}$$

Equation (36) clearly shows that the symmetric Trotter factorization of the propagator in Eq. (35) amounts to a midpoint time discretization for $\exp[\Delta t i\mathcal{L}^L(t)]$. Different ordered break-up of the propagator, in Eq. (32), using the Trotter formula would result in different discretization recipes in Eq. (36). If Δt is sufficiently small the propagator in Eq. (35) can be approximated as

$$\begin{aligned}\mathcal{U}^L_{\alpha_{j-1}\alpha'_{j-1},\alpha_j\alpha'_j}(\Delta t,0)=e^{\Delta t\mathcal{I}}\mathcal{W}_{\alpha_{j-1}\alpha'_{j-1}}(t_{j-1},t_j)&\\\times e^{\Delta t i L^L_{\alpha_{j-1}\alpha'_{j-1}}(\Delta t/2)}(\delta_{\alpha_{j-1}\alpha_j}s\,\delta_{\alpha'_{j-1}\alpha'_j}&\\-\Delta t J_{\alpha_{j-1}\alpha'_{j-1},\alpha_j\alpha'_j}).&\end{aligned} \tag{37}$$

Equation (37) is the propagator that may be used for evolution in a single time step in the sequential short-time propagation algorithm. Starting from Eq. (37) the implementation of the algorithm proceeds as described in Refs. 14 and 18.

B. Numerical integration of Langevin dynamics

The action of the time-dependent operator $L^L_{\alpha\alpha'}(t)$ [Eq. (13)] appearing in the single time slice propagator in Eq. (37) generates trajectory segments following Langevin dynamics according to Eqs. (9) and (10). So one has to employ a suitable scheme to integrate numerically the Langevin stochastic differential equations of motion.

A number of schemes to perform such stochastic integrations exist. In particular, algorithms have been proposed using the Runge–Kutta integrator[22,23] and the velocity Verlet integrator.[24] Here we discuss a low-order scheme derived from the factorization of the time-dependent propagator in Suzuki's approach.[20,25]

The time-dependent Langevin–Liouville operator in Eq. (13) can be decomposed as $L^L(t)=L^L_1+L^L_2+L^L_3+L^L_4(t)$ where

$$L^L_1=P\frac{\partial}{\partial R}, \tag{38}$$

$$L^L_2=(\mathcal{F}^\alpha_W+\mathcal{F}^{\alpha'}_W)\frac{\partial}{\partial P}, \tag{39}$$

$$L^L_3=-\zeta P\frac{\partial}{\partial P}, \tag{40}$$

$$L^L_4(t)=\xi(t)\frac{\partial}{\partial P}. \tag{41}$$

The Langevin propagator, defined by the time-ordered exponential in Eq. (14), can be factorized using a symmetric Trotter formula using Suzuki's[20] approach as

$$\begin{aligned}U(\tau)=e^{(\tau/2)\mathcal{I}}e^{(\tau/2)L^L_4(\tau)}e^{(\tau/2)L^L_3}e^{(\tau/2)L^L_2}e^{\tau L^L_1}e^{(\tau/2)L^L_2}&\\\times e^{(\tau/2)L^L_3}e^{(\tau/2)L^L_4(\tau)}e^{(\tau/2)\mathcal{I}}.&\end{aligned} \tag{42}$$

A numerical algorithm to propagate the phase space point along the trajectory segments can be easily derived using Eq. (42) along the lines described in Refs. 26 and 27. The algorithm is correct only to order $\mathcal{O}(\tau^{3/2})$ but, using an integration step $\tau=1\times10^{-2}$ in scaled units, the scheme has been shown to be sufficient for the calculation of the short trajectory segments needed to the compute the rate constants.

VI. RESULTS

A. Adiabatic dynamics

In the adiabatic limit only the species variables A and B need to be considered and the rate constant k_{AB} suffices to describe the chemical kinetics. Thus we need to evaluate Eq. (29) using adiabatic dynamics on the ground-state surface for which $N_B(R,P,t)=N_B(R(t),P(t))$. In Fig. 2 we show the phase space (R,P) sampled by adiabatic dynamics on the ground adiabatic surface (11) in an ensemble of 5×10^4 trajectories for $\beta=6$ and $\zeta=1$. This figure shows the expected

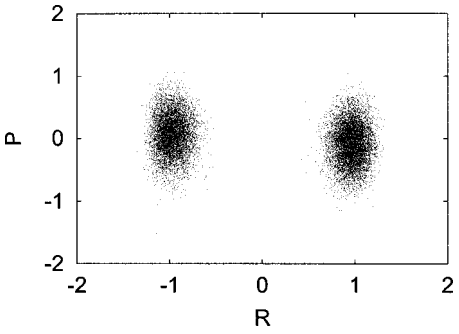

FIG. 2. Phase space (R,P) sampled by adiabatic dynamics on the ground adiabatic surface (11) in an ensemble of 5×10^4 trajectories for $\beta=6$ and $\zeta=1$.

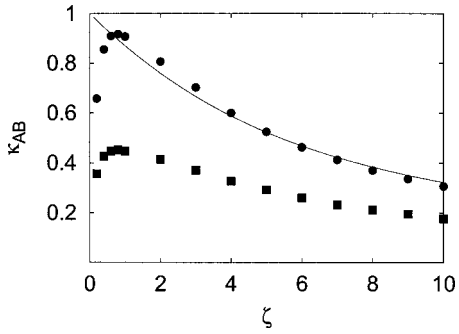

FIG. 4. Adiabatic transmission coefficient κ_{AB} (black circles) as function of ζ for $\beta=6$. Nonadiabatic results including up to six transitions (black squares). The solid line is a plot of Kramers' formula.

concentration of phase space points around the two minima with small density around $R=0$, typical of an activated rate process.

While keeping $\beta=6$ fixed we have performed calculations for $\zeta=1,\ldots,10$. In order to study Kramers crossover regime we have also considered low values of the friction, $\zeta=0.2,0.4,0.6,0.8$. The transition state result is independent of the friction ζ and its calculated value is $k_{AB}^{TST}=4.5\times10^{-5}$. In Fig. 3 we show the time-dependent transmission coefficient $\kappa_{AB}(t)=k_{AB}(t)/k_{AB}^{TST}$ for $\zeta=0.2$, 5, and 8. Note that for low friction $\zeta=0.2$ the time-dependent transmission coefficient has structure at short times before the plateau is established. We have used 5×10^5 trajectories to sample the phase space to achieve a statistical error of 1% for ten different values of ζ. In Fig. 4 we show the dependence of the adiabatic transmission coefficient κ_{AB} on the friction ζ. We compare our numerical results with Kramers' formula $\kappa_{AB}^{K}=\omega_{\max}^{-1}(\sqrt{\zeta^2/4+\omega_{\max}^2}-\zeta/2)$. In order to fit of our numerical results we have set $\omega_{\max}=3.6$ in the theoretical formulas. This value should be compared with the high frequency at the barrier top ($\omega_b=178.77$) which is due to the "pimple" in the adiabatic ground-state energy at $R=0$ (not easily discerned on the resolution of Fig. 1) which arises from the near avoided crossing with the excited state curve. The value $\omega_{\max}=3.6$ is consistent with the curvature of the ground-state profile at the barrier top, excluding the "pimple." In Fig. 4 we see that the Kramers expression agrees well with the adiabatic simulation results for high friction but, as expected, does not capture the turnover at small values of ζ.

B. Nonadiabatic dynamics

Nonadiabatic dynamics accounts for the possibility of transitions to the excited-state surface and the mean of the excited- and ground-state surfaces using the algorithm discussed above. We have used 10^6 trajectories to sample phase space and considered up to six quantum transitions (we have verified the convergence of our results by calculating up to eight nonadiabatic transitions). In Fig. 5 we show F_n the fraction of trajectories in the ensemble involving $n=0,1,2,3,4,5,6$ transitions versus time. This figure shows the importance of nonadiabatic transitions for times $t>0$ and the decreasing importance of the dynamics with large numbers of nonadiabatic transitions within the time interval displayed in the figure.

In Fig. 6 we show the phase space (R,P) sampled by nonadiabatic dynamics including up to $n=6$ quantum transitions in an ensemble of 5×10^4 trajectories starting and ending in the ground state (11) for $\beta=6$ and $\zeta=1$. In contrast to Fig. 2 for adiabatic dynamics, one sees additional density in the vicinity of $R=0$ reflecting effects arising from transitions to the excited state. Note also the distribution of phase space points corresponding to positive (negative) momenta leading to species A (B).

Using the ensemble of 10^6 trajectories to compute $k_{AB}^{d}(t)$ we have obtained a statistical error of the same order of magnitude as that in the adiabatic calculation. The contributions coming from $k_{AB}^{o1}(t)$ and $k_{AB}^{o2}(t)$ are zero within the

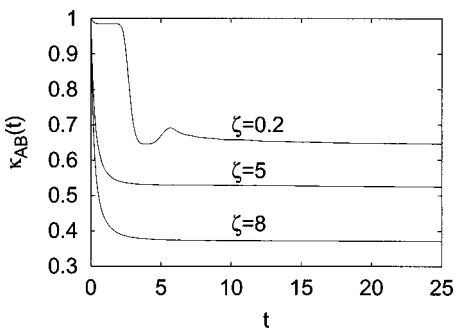

FIG. 3. Transmission coefficient for $\beta=6$ and three different values of ζ. The upper curve is for $\zeta=0.2$, the middle curve for $\zeta=5$, and the lowest curve for $\zeta=8$.

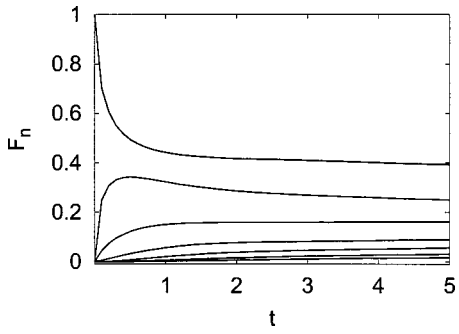

FIG. 5. The fraction of trajectories in the ensemble F_n vs time for a calculation involving $n=0,1,2,3,4,5,6$ quantum transitions. The upper curve is for $n=0$ then, in descending order, the remaining curves are for higher values of n with the lowest curve corresponding to $n=6$.

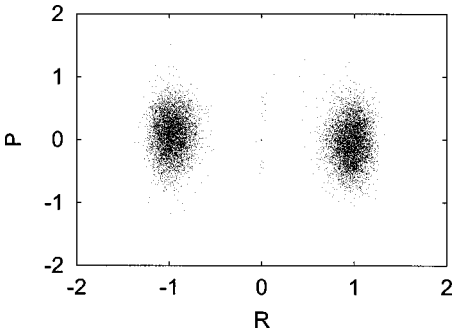

FIG. 6. Phase space (R,P) sampled by nonadiabatic dynamics including up to $n=6$ quantum transitions in an ensemble of 5×10^4 trajectories starting and ending in the ground state (11) for $\beta=6$ and $\zeta=1$.

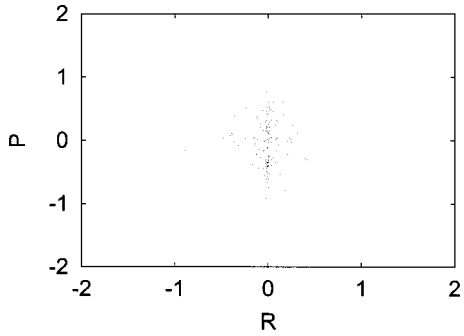

FIG. 8. Phase space (R,P) sampled by nonadiabatic dynamics including up to $n=6$ quantum transition in an ensemble of 5×10^4 trajectories starting from the coupled surface (12) and ending in the state (22) for $\beta=6$ and $\zeta=5$.

statistical error. The convergence of the calculation κ_{AB} with respect to the number of nonadiabatic transitions is shown in Fig. 7.

Figure 4 summarizes the results for the nonadiabatic transmission coefficients as a function of the friction. One sees a substantial decrease in κ_{AB} since nonadiabatic transitions provide an additional recrossing mechanism. The effects are even more pronounced for low and intermediate values of the friction.

For nonadiabatic dynamics the rate k_{AC} also comes into play. In Fig. 8 we show the phase space points involved in the calculation of the main contribution to k_{AC} for $\zeta=5$. The configuration space points are sampled uniformly on the right side of the coupled surface in Fig. 1 and the trajectories include up to $n=6$ quantum transitions and must end on the excited (22) surface after a time $t=5$. One again sees a concentration of phase space points near $R=0$ and the distribution of points reflects the single well character of the excited-state potential-energy curve.

Figure 9 shows the time-dependent rate coefficient $k_{AC}(t)$ for $\beta=2$ and $\zeta=1$,5, and 10. The main contribution comes from k_{AC}^{o2} with k_{AC}^{d} and k_{AC}^{o1} zero within the statistical error. Since this rate constant has no classical analog it has a structure typical of quantum rate processes. It starts a zero at $t=0$ and rises to form a plateau at long times. Its value is quite small and for low friction ($\zeta=1$) a well defined rate process is not established. The statistical errors are much larger for the calculation of this rate constant.

VII. CONCLUSIONS

We have shown how correlation function expressions for rate constants can be computed for a quantum-classical system embedded in a dissipative environment. The rate constants are determined by nonadiabatic evolution of microscopic species variables expressed in terms of surface-hopping Langevin trajectories. The sequential short-time propagation algorithm has proved to be very effective for the computation of the correlation functions involved in rare reactive dynamics and is to be preferred to the Dyson formalism used in our earlier study of nonadiabatic reaction rates in the context of deterministic quantum-classical dynamics.[10]

While explicit calculations have been performed for a simple two-level system coupled to a quartic potential in a dissipative environment, the methods we have developed can be used to study arbitrary quantum-classical subsystems in dissipative environments. The stochastic algorithms discussed in this paper are directly applicable to these more complicated cases. Consequently, the methods developed and illustrated in this paper should provide the tools needed to investigate realistic models where the detailed dynamics of a portion of the environment is not important and can be treated as a stochastic heat bath.

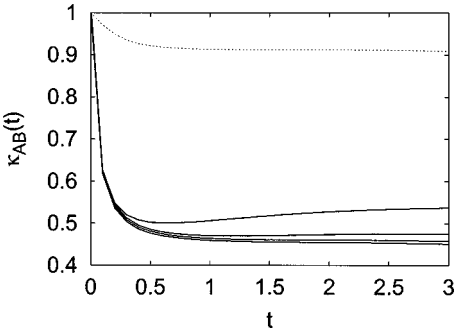

FIG. 7. Transmission coefficient for $\beta=6$ and $\zeta=1$. The upper dotted curve shows the adiabatic result $n=0$ and, in descending order, the solid curves are for $n=2$, 4, 6, and 8. The curves for $n=6$ and $n=8$ are not distinguishable within the statistical error.

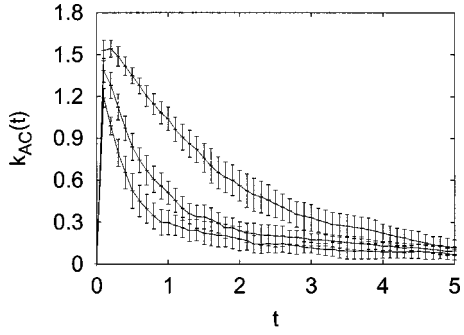

FIG. 9. Time-dependent rate coefficient $k_{AC}(t)$ for $\beta=6$. The upper curve is for $\zeta=1$, the middle curve for $\zeta=5$, and the lower curve is for and $\zeta=10$. The error bars indicate ±1 standard deviation. The y axis is in units of 10^{-5}.

APPENDIX: STATIONARY DENSITY MATRIX OF THE QUANTUM-CLASSICAL SYSTEM IN THE BATH

An important element in the calculation of correlation functions at equilibrium is the density matrix which is stationary under the Liouville operator defining the dynamics of the system.[10] The stationary density matrix for a general quantum-classical system has been derived in Ref. 9. Here we derive the stationary density matrix $\hat{\rho}_{We}$ for the dissipative quantum-classical Liouville operator Eq. (1) which satisfies $-i\mathcal{L}^D\hat{\rho}_{We}=0$. To find $\hat{\rho}_{We}$ we follow Ref. 9 and consider the expansion of the density matrix in powers of $\hbar$,

$$\hat{\rho}_{We}=\sum_{n=0}^{\infty}\hbar^n\hat{\rho}_{We}^{(n)}. \tag{A1}$$

We seek an explicit solution in the adiabatic basis. Using the expansion of the density matrix in powers of $\hbar$ the stationary condition is equivalent to an infinite set of equations corresponding to the various powers of $\hbar$:

$$iE_{\alpha\alpha'}\rho_{We}^{(0)\alpha\alpha'}=0, \tag{A2}$$

$$iE_{\alpha\alpha'}\rho_{We}^{(n+1)\alpha\alpha'}=\sum_{\beta\beta'}-i\mathcal{L}^K_{\alpha\alpha'\beta\beta'}\rho_{We}^{(n)\beta\beta'}+\sum_{\beta\beta'}J_{\alpha\alpha',\beta\beta'}\rho_{We}^{(n)\beta\beta'}\quad(n\geqslant 1). \tag{A3}$$

As discussed in Ref. 9, to ensure that solution can be found by recursion one must discuss the solution of Eq. (A3) when calculating the diagonal elements $\rho_{We}^{(n)\alpha\alpha}$ in terms of the off-diagonal ones $\rho_{We}^{(n)\alpha\alpha'}$. To this end, using $\rho_{We}^{(n)\alpha\alpha'}=(\rho_{We}^{(n)\alpha'\alpha})^*$, $J_{\alpha\alpha,\beta\beta'}=J^*_{\alpha\alpha,\beta'\beta}$ and the fact that $J_{\alpha\alpha,\beta\beta}=0$ when a real basis is chosen, it is useful to rewrite Eq. (A3) in the form

$$iL^K_{\alpha\alpha}\rho_{We}^{(n)\alpha\alpha}=\sum_{\beta>\beta'}2\mathcal{R}(J_{\alpha\alpha,\beta\beta'}\rho_{We}^{(n)\beta\beta'}). \tag{A4}$$

In the present case the left-hand side of Eq. (A4) is not a self-adjoint operator and it does not have a Poisson bracket form. In order to find a solution to Eq. (A4), the theorem of Fredholm alternatives requires that the null space of the adjoint operator $iL^{K,B}_{\alpha\alpha}$ must be orthogonal to the right-hand side of Eq. (A4). The second term of the left-hand side of Eq. (A4) is dissipative in character so that neither H^α_W is a constant of motion nor is any general function $f(H^\alpha_W)$. However we can consider the left eigenvalue of $iL^K_{\alpha\alpha}$ which is any constant number $\mathcal{C}$ so that the condition of orthogonality becomes

$$\int dRdP\sum_{\nu>\nu'}2\mathcal{R}(J_{\alpha\alpha,\nu\nu'}\rho_{We}^{(n)\nu\nu'})\mathcal{C}=0. \tag{A5}$$

Due to the fact that J is an odd function of momenta, Eq. (A5) is satisfied if one assumes that $\rho_{We}^{(n)\nu\nu'}$ is an even function of momenta. To first order in $\hbar$ the results are the same for deterministic quantum-classical dynamics and are given in the text.

[1] P. Hänggi, P. Talkner, and M. Borkovec, Rev. Mod. Phys. **62**, 251 (1990).
[2] D. Kohen, C. C. Marston, and D. J. Tannor, J. Chem. Phys. **107**, 5236 (1997).
[3] M. Topaler and N. Makri, J. Chem. Phys. **101**, 7500 (1994); J. Phys. Chem. **100**, 4430 (1996).
[4] J.-L. Liao and E. Pollak, J. Chem. Phys. **116**, 2718 (2002).
[5] E. Sim, G. Krilov, and B. J. Berne, J. Phys. Chem. A **105**, 2824 (2001).
[6] J. Casado-Pascual, C. Denk, M. Morillo, and R. I. Cukier, J. Chem. Phys. **113**, 11176 (2000).
[7] R. E. Cline, Jr. and P. G. Wolynes, J. Chem. Phys. **86**, 3836 (1987); D. F. Coker, H. S. Mei, and J. P. Ryckaert, in *Classical and Quantum Dynamics in Condensed Matter Simulations*, edited by B. J. Berne, G. Ciccotti, and D. F. Coker (World Scientific, Singapore, 1998), p 539.
[8] R. Kapral and G. Ciccotti, J. Chem. Phys. **110**, 8919 (1999).
[9] S. Nielsen, R. Kapral, and G. Ciccotti, J. Chem. Phys. **115**, 5805 (2001).
[10] A. Sergi and R. Kapral, J. Chem. Phys. **118**, 8566 (2003).
[11] E. B. Davis, *Quantum Theory of Open Systems* (Academic, London, 1976).
[12] U. Weiss, *Quantum Dissipative Systems* (World Scientific, Singapore, 1999).
[13] R. Kapral, J. Phys. Chem. A **105**, 2885 (2001).
[14] D. Mac Kernan, G. Ciccotti, and R. Kapral, J. Phys.: Condens. Matter **14**, 9069 (2002).
[15] D. Mac Kernan, G. Ciccotti, and R. Kapral, J. Chem. Phys. **116**, 2346 (2002).
[16] C. W. Gardiner, *Handbook of Stochastic Methods* (Springer, New York, 2002), 2nd ed.
[17] A. Sergi, D. Mac Kernan, G. Ciccotti, and R. Kapral, Theor. Chem. Acc. **110**, 49 (2003).
[18] R. Kapral and G. Ciccotti, in *Bridging Time Scales: Molecular Simulations for the Next Decade*, 2001, edited by P. Nielaba, M. Mareschal, and G. Ciccotti (Springer, Berlin, 2003), p. 445.
[19] In the implementation of the momentum-jump approximation we have removed from the ensemble trajectories with a high momentum jump $\delta P > \hat{d}_{\alpha_j\alpha_k}\delta P_{cut}$. In our calculations we have used $\delta P_{cut}=2$.
[20] M. Suzuki, Proc. Jpn. Acad., Ser. B: Phys. Biol. Sci. **69**, 161 (1993).
[21] H. F. Trotter, Proc. Am. Math. Soc. **10**, 545 (1959).
[22] E. Helfand, J. Chem. Phys. **69**, 1010 (1978).
[23] E. Helfand, Bell Syst. Tech. J. **58**, 2289 (1978).
[24] W. F. Van Gusteren, H. J. C. Berendsen, and J. A. C. Rullmann, Mol. Phys. **44**, 69 (1981).
[25] A. Ricci and G. Ciccotti, Mol. Phys. **101,** 1927 (2003).
[26] M. Tuckerman, B. J. Berne, and G. J. Martyna, J. Chem. Phys. **97**, 1990 (1992).
[27] A. Sergi, M. Ferrario, and D. Costa, Mol. Phys. **97**, 825 (1999).